Zdeněk P. Bažant
McCormick School Professor
and W.P. Murphy Professor
Fellow ASME
Department of Civil and Environmental
Engineering,
Northwestern University,
2145 Sheridan Road, CEE/A135,
Evanston, IL 60208
e-mail: z-bazant@northwestern.edu

Yong Zhou[1]
Graduate Research Assistant
Department of Civil and Environmental
Engineering,
Northwestern University,
Evanston, IL 60208

Isaac M. Daniel
W.P. Murphy Professor
Fellow ASME
Department of Civil and Environmental
Engineering,
Northwestern University,
2145 Sheridan Road, CEE/A135,
Evanston, IL 60208
e-mail: imdaniel@northwestern.edu

Ferhun C. Caner[2]
Visiting Scholar
Northwestern University,
Evanston, IL 60208

Qiang Yu
Graduate Research Assistant
Department of Civil and Environmental
Engineering,
Northwestern University,
Evanston, IL 60208

Journal of Engineering Materials and Technology
Vol. 28 (No.3) 2006
pp. 366-374

Size Effect on Strength of Laminate-Foam Sandwich Plates

Experiments on size effect on the failure loads of sandwich beams with PVC foam core and skins made of fiber-polymer composite are reported. Two test series use beams with notches at the ends cut in the foam near the top or bottom interface, and the third series uses beams without notches. The results demonstrate that there is a significant nonstatistical (energetic) size effect on the nominal strength of the beams, whether notched or unnotched. The observed size effect shows that the failure loads can be realistically predicted on the basis of neither the material strength concept nor linear elastic fracture mechanics (LEFM). It follows that nonlinear cohesive (quasi-brittle) fracture mechanics, or its approximation by equivalent LEFM, must be used to predict failure realistically. Based on analogy with the previous asymptotic analysis of energetic size effect in other quasibrittle materials, approximate formulas for the nominal strength of notched or unnotched sandwich beams are derived using the approximation by equivalent LEFM. Different formulas apply to beams with notches simulating pre-existing stress-free (fatigued) cracks, and to unnotched beams failing at crack initiation. Knowledge of these formulas makes it possible to identify from size effect experiments both the fracture energy and the effective size of the fracture process zone. [DOI: 10.1115/1.2194557]

Introduction

According to current practice and all textbooks, sandwich plates and shells are generally designed under the hypothesis that material failure is determined by the concept of material strength, based on either plastic limit analysis or elasticity with a strength limit [1–10]. This practice implies that there is no deterministic size effect. However, recent experiments at Northwestern University demonstrate that sandwich components, such as the fiber-polymer composites [11–14] and polymeric foams [15], usually fail in a brittle manner and exhibit strong deterministic size effect, calling for the use of fracture mechanics. Naturally, the same must be expected for the failure of sandwich plates.

The size effect is particularly important for designing large sandwich structures, contemplated for the construction of hulls, decks, bulkheads, masts, and antenna covers of large ships, and of large load-bearing fuselage panels, vertical stabilizer, rudder, wing box, and other components of future aircraft.

The objective of this study is to investigate the size effect in sandwich plates, both experimentally and analytically. A numerical indication of size effect in sandwich plates with a limited size range has recently been reported [16].

Laminate-foam sandwich plates can fail in a variety of modes, including [17]: (1) the debonding shear fracture of skins (or face sheets), (2) fracture in the foam core, (3) compression fracture of skins [18], (4) delamination with skin buckling, (5) skin wrinkling [19], and (6) foam core indentation. These modes often interact. The first three modes must, in principle, lead to deterministic size effects. So probably does the fourth, as well as the fifth if it leads to cohesive delamination. This study is focused particularly on the first two. Experiments have been designed so as to obtain failure in one or both of these two modes.

Some previous studies treated skin debonding in terms of fracture mechanics [20,21]. However, the analysis has been confined to linear elastic fracture mechanics (LEFM), in which the fracture process zone (FPZ) is considered to be shrunken into a point. Recent size effect experiments on fiber-polymer laminates and on polyvinyl chloride (PVC) foam, conducted at Northwestern Uni-

[1]Currently Assistant Professor, Department of Building Engineering, Tongji University, Siping Road 1239, Shanghai, China; e-mail: yongzhou@mail.tongji.edu.cn

[2]Ramón y Cajal Researcher and Lecturer on leave from UPC (ETSECCPB, Campus Nord), Jordi Girona 1-3, Edif. D2, E-08034 Barcelona, Spain; e-mail: ferhun.caner@upc.edu

Contributed by the Materials Division of ASME for publication in the JOURNAL OF ENGINEERING MATERIALS AND TECHNOLOGY. Manuscript received September 28, 2004; final manuscript received December 29, 2005. Review conducted by Ann Marie Sastry.

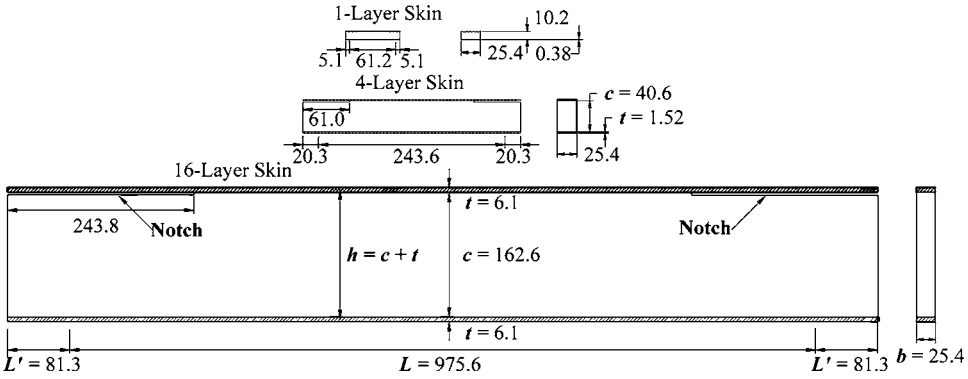

Fig. 1 Dimensions of test beams with notches on top

versity [13,15] reveal that the size effect is weaker than the power-law size effect of LEFM. This implies quasibrittle behavior in which the FPZ size is not negligible.

Therefore, this study will consider the FPZ to be finite. The finiteness of FPZ will be approximately captured by adopting the equivalent LEFM—a theory in which the tip of an equivalent LEFM crack is placed into the middle of the FPZ, considered to have a certain finite length, denoted as $2c_f$. The analysis will draw on analogy with previous size effect studies of many other quasi-brittle materials [22–29].

Size Effect Tests of Sandwich Beams with Foam Core

The cores of all sandwich beams were made of closed cell PVC foam with mass density 100 kg/m^3 (25.4 mm thick sheets of Divinycell H100, procured from Diabgroup, Inc.). The properties of the foam (as specified by the supplier) were as follows: tensile elastic modulus 105 MPa, tensile strength 3.1 MPa, compressive elastic modulus 130 MPa, compressive strength 1.7 MPa, elastic shear modulus 40 MPa, and shear strength 1.4 MPa.

To investigate the size effect, beams geometrically scaled in two dimensions were fabricated. The beams of all three sizes had the same width: $b=25.4$ mm. All of the cores were cut from the same sheet of foam. The thickness t of the skins was scaled in proportion to the core depth c. Three series of tests were carried out. The scaling ratios were 1: 4: 16 for series I and 1: 3: 9 for series II and III. For series III, the beams had no notches. For series I and II, notches were cut in the foam as close as possible to the interface with the top or bottom skin, respectively, but without cutting into the skin, and without baring it. The notches in series I and II were symmetric, cut at both ends of the beam (Fig. 1). The distance a of each notch tip from the support axis was equal to core depth c. Each notch tip was sharpened by a razor blade of 0.25 mm thickness. The purpose of making the notches was to clarify the effect of large pre-existing cracks or damage zones, and to force the fracture to develop at a certain predetermined location, homologous (geometrically similar) for all the sizes. The notches also helped to avoid a conceivable Weibull-type statistical contribution to the size effect. The choice of beam and notch proportions was also guided by the need to prevent significant core indentation, which would complicate interpretation of the results. Furthermore, the notches made it possible to obtain shear fracture for a relatively small length-depth ratio of the test beams. All the beams were subjected to three-point loading.

Test Series I, with Fiberglass-Epoxy Skins and Notches at Top Interface. The skins consisted of a cured woven glass-epoxy composite (FS-12A, procured from Aerospace Composite Products, as 0.38 mm thick sheets). The following properties were obtained through material tests: longitudinal elastic modulus 30 GPa, transverse modulus 28 GPa, transverse strength 300 MPa, in-plane shear modulus 5 MPa, and in-plane shear strength 90 MPa. The depths of the foam cores were $c=10.2$, 40.6, and 162.6 mm (Figs. 1 and 2(a)). The scaling of the skin thicknesses was achieved by bonding 25.4 mm wide composite strips—one strip for the smallest beams, four strips for the medium beams, and 16 strips for the largest beams. The ratio of L/c was almost 6:1 for all the beams (and thus the effective lengths of the beams were $L=61.2$, 243.6, and 975.6 mm). All the beams of series I were loaded in an Instron 5000 universal testing machine.

Local failure under the corners of loading platens is a sensitive aspect. It could be so extensive as to control the maximum load. This problem was avoided by placing two separate rubber sheets on top of the skin. Furthermore, between these sheets and the metallic platen (aluminum for series I, and steel for series II and III), two laminate plates (consisting of the same material as the skins) were inserted (having dimensions $10\times25.4\times6$ mm, $40\times25.4\times6$ mm, and $160\times25.4\times6$ mm for series I, and $17\times25.4\times4.8$ mm, $51\times25\times4.8$ mm, and $154\times25.4\times4.8$ mm for series II and III). Observations showed that a small crack grew in the top laminate plate from the edge of the platen, but did not extend into the second laminate plate.

Figure 2(b) shows the failure of a medium size beam. To ensure that the viscoelastic and loading rate effects in the foam, skins, and FPZ were similar for beams of different sizes, the cross-head speed was set so as to make all the specimens reach the peak load within about the same time, chosen as 5 min.

Figure 3(a) shows, for all three sizes, typical records of the load-deflection curves up to failure. It is obvious that, the larger the specimen, the more brittle its response. For example, in the

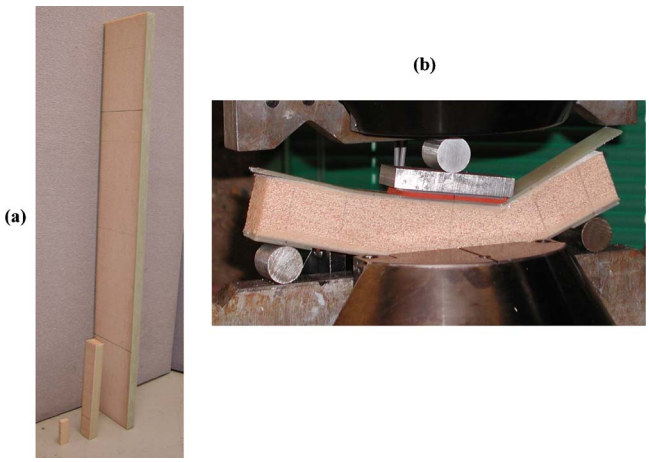

Fig. 2 (a) Photo of top-notched test beams of all three sizes and (b) photo of top-notched beam of medium size during the test

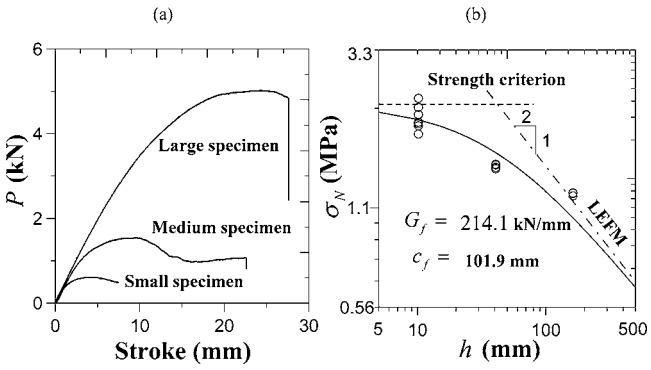

Fig. 3 (*a*) Load-deflection diagrams measured on top-notched beams of three sizes and (*b*) nominal strength values of these beams compared to the classical energetic size effect law

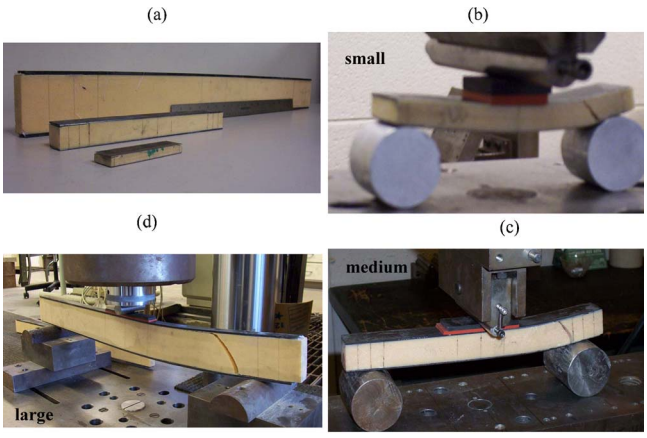

Fig. 5 (*a*) Photo of bottom-notched test beams of all three sizes; and (*b*, *c*, *d*) photos of typical failure modes of bottom-notched beams for each of three sizes

largest specimen, crack propagation becomes unstable and the load suddenly drops right after the peak load, while in the smallest specimen, and to a lesser extent also in the medium specimen, one can see a period of gradual post-peak softening. In the largest specimen, the loss of crack growth stability after the peak is manifested by a loud noise, while in the medium size specimen one hears several quieter sound emissions during the gradual post-peak decline of load.

The measured maximum loads P are listed in Table 1. Fig. 3(*b*) shows a plot of the measured values of nominal strength

$$\sigma_N = P/bD \tag{1}$$

where D=characteristic structure (or specimen) size, in our case taken equal to the beam depth, $D=h$, and $h=c+t$=distance between skin centroids, chosen as the characteristic beam size. We see that there is a strong size effect but must notice that, in contrast to the other size effect tests, the size effect trend of the data obtained exhibits a positive curvature. If this were a systematic trend, it might be attributed to the fact that the top skin is subjected to compression force causing a skin wrinkling instability [30,36,37] and mixed mode fracture with a nonzero mode I component for which the fracture energy is much less than for mode II. However, calculations have shown such instability to be impossible because the critical load is much higher than the loads recorded. Thus, the positive curvature in Fig. 3(*b*) is likely a chancy event.

Table 1 Data and test results for beams with notches on top

No.	Depth c (mm)	Width b (mm)	Length L (mm)	Load P (N)	σ_N (MPa)
S1	10.2	25.4	61.2	507.01	1.887
S2	10.2	25.4	61.2	478.72	1.781
S3	10.2	25.4	61.2	516.14	1.921
S4	10.2	25.4	61.2	548.90	2.043
S5	10.2	25.4	61.2	547.62	2.038
S6	10.2	25.4	61.2	614.28	2.286
S7	10.2	25.4	61.2	519.24	1.932
S8	10.2	25.4	61.2	519.10	1.932
M1	40.6	25.4	243.6	1517.03	1.418
M2	40.6	25.4	243.6	1550.52	1.449
M3	40.6	25.4	243.6	1543.12	1.442
M4	40.6	25.4	243.6	1547.92	1.447
M5	40.6	25.4	243.6	1502.86	1.405
L1	162.6	25.4	975.6	5081.78	1.186
L2	162.6	25.4	975.6	4984.72	1.163
L3	162.6	25.4	975.6	5066.60	1.182

The size effect in sandwich beams with notches at the bottom skin-foam core interface is also of interest because it is probable that the failure mechanism is different in such beams compared to the beams with notches at the top interface. Therefore, a second test series has been carried out, with notches near the bottom skin, which is subjected to tension.

Test Series II, with Carbon-Epoxy Skins and Notches at Bottom Interface. The foam cores were the same as in Series I. However (for no other reason than convenient availability), a different material was used for the skins—unidirectional carbon-epoxy (IM6-G/3501-6, provided by Hexcel, Inc., in a 12 in. wide roll, with along the fiber Young's modulus measured as 172 GPa). The prepregs material was cut into 12×12 in. sheets for the small and medium specimens, and 34×10 in. sheets for the large specimens. Next, for small, medium and large specimens (Figs. 4 and 5(*a*)), respectively, 3, 9, and 27 layers of prepreg sheets were laid up. The 12×12 in. laminates were cured in a compression-lamination press (Tetrahedron MTP-14), while the 34×10 in. laminates were cured in an autoclave (McGrill). The curing pro-

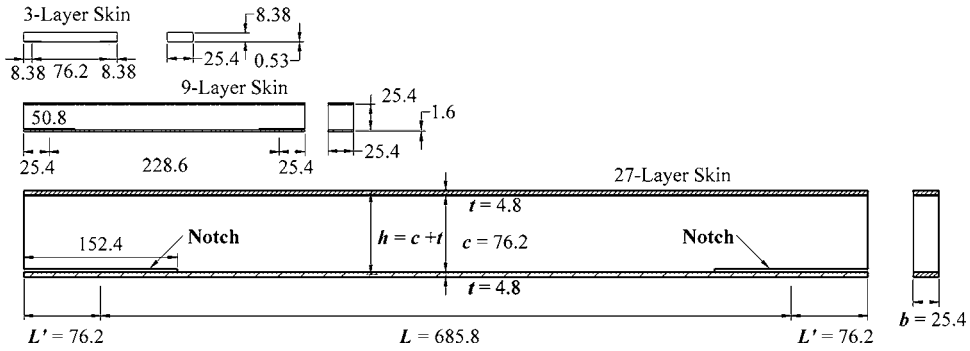

Fig. 4 Dimensions of test beams with notches at bottom

Table 2 Data and test results for beams with notches at bottom

No.	Depth c (mm)	Width b (mm)	Length L (mm)	Load P (KN)	σ_N (MPa)
S1	8.5	25.4	76.2	0.795	3.477
S2	8.5	25.4	76.2	0.793	3.468
S3	8.5	25.4	76.2	0.844	3.692
S4	8.5	25.4	76.2	0.786	3.438
S5	8.5	25.4	76.2	0.804	3.517
S6	8.5	25.4	76.2	0.759	3.320
S7	8.5	25.4	76.2	0.805	3.521
M1	25.4	25.4	228.6	2.283	3.328
M2	25.4	25.4	228.6	1.914	2.790
M3	25.4	25.4	228.6	1.837	2.678
M4	25.4	25.4	228.6	2.273	3.314
M5	25.4	25.4	228.6	1.693	2.468
L1	76.2	25.4	685.8	3.984	1.936
L2	76.2	25.4	685.8	3.319	1.613
L3	76.3	25.4	685.8	3.420	1.662
L4	76.3	25.4	685.8	3.690	1.793

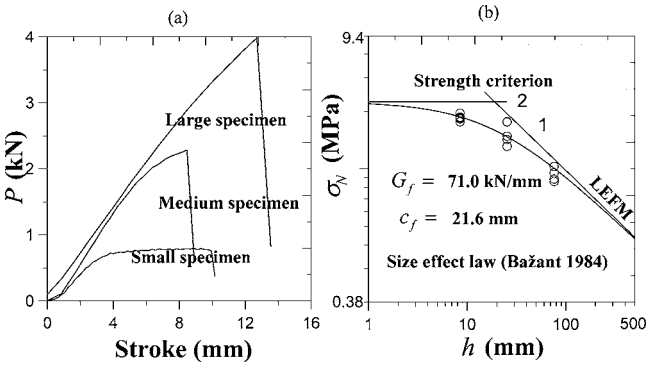

Fig. 6 (*a*) Load-deflection diagrams measured on bottom-notched beams of three sizes and (*b*) nominal strength values measured on these beams of three sizes, compared to the classical energetic size effect law

cess suggested by the manufacturer for the 3501-6 epoxy matrix was followed (it involved a maximum curing temperature of 350°F and a maximum curing pressure of 75 psi). After curing, the laminates were cut into 3.67×1.0 11.0×1.0, and 33.0×1.0 in. strips, by means of a diamond saw. The thicknesses of the $[0]_3$, $[0]_9$, and $[0]_{27}$ laminate skins were 0.021, 0.063, and 0.189 in. (0.53, 1.60, and 4.80 mm) for the small, medium, and large specimens, respectively. The foam (Divinycell H100) was cut into $3.67\times0.33\times1.0$, $11.0\times1.0\times1.0$, and $33.0\times3.0\times1.0$ in. ($93.2\times8.4\times25.4$, $279.6\times25.4\times25.4$, $839.0\times76.2\times25.4$ mm) blocks for the small, medium, and large specimens, respectively. The ratio of L/c of these beams was 9:1, and thus the effective beam lengths were 3, 9, and 27 in., or 76.2, 228.6, and 685.8 mm, respectively (Figs. 4 and 5).

The skins and foam cores were bonded together by epoxy adhesive and were cured in a vacuum bag for 8 h.

The small and medium specimens were tested under three-point bending in a universal testing machine (MTS, 20 kip), while the large specimens were tested in a larger machine (MTS 220 kip) because of their large dimensions rather than strength. The loading rate was chosen so as to reach the peak load of the specimens of all sizes within about 3 min.

For all the specimens, without exception, the final failure mode observed after the load dropped was diagonal tensile fracture which propagated through the foam (Figs. 5(*b*)–5(*d*)). Whether the diagonal tensile fracture in the foam occurred at or before the peak load was not recorded. Preliminary finite element simulations indicate that, for large-size beams it surely happened after the peak load, and probably also for the medium and small size beams. Consequently, the failure modes may be assumed to be geometrically similar. In addition, the tests confirmed that the larger the specimen, the greater the brittleness of response, as revealed by post-peak behavior.

The measured maximum loads P are listed in Table 2. The load-deflection curves for all three specimen sizes are shown in Fig. 6(*a*), and the measured variation of nominal strength $\sigma_N = P/bh$ is plotted in Fig. 6(*b*).

Test Series III, with Carbon-Epoxy Skins and No Notches. The beams of test series III were the same as in series II, except that the foam block dimensions were $3.67\times0.25\times1.0$, $11.0\times0.75\times1.0$, and $33.0\times2.25\times1.0$ in. ($93.2\times6.4\times25.4$, $279.6\times19.0\times25.4$, and $839.0\times57.2\times25.4$ mm), which means that the ratio of L/c was 12: 1. In addition, the notches were absent (Figs. 7 and 8(*a*)). The scaling ratios of the length and depth dimensions of all the beams were 1: 3: 9 (Fig. 7).

In series III, the failure modes varied. In the small beams, no diagonal shear fracture was observed and the failure was caused by compressive fracture of the upper skin. This mode of failure was also observed in some medium and large beams, but in most of these beams the interface crack branched into a diagonal tensile crack which crossed the foam core (Figs. 8(*b*)–8(*d*)). A size effect was found again, but it was not as strong as in the notched beams.

The measured maximum loads P are listed in Table 3. The load-deflection curves for the beams of all three sizes are shown in Fig. 9(*a*), and the measured variation of nominal strength σ_N with size h is plotted in Fig. 9(*b*).

Simplified Analysis of Fracture and Size Effect

If the strength theory or plastic limit analysis were applicable to sandwich beams, a size effect would have to be absent, and thus the mean trend of the size effect plots in Figs. 3(*b*), 6(*b*), and 9(*b*) would have to be horizontal. This is obviously not the case. Because, in the notched beams, fracture can begin propagating at only one place—the notch tip—the fact that other points may have a lower random strength must be immaterial. This means that, in notched beams, the Weibull-type statistical size effect is impossible. So it is for the unnotched beams of series III, because their fracture, too, begins always at the same place—at the interface at the beam end. Hence, any observed size effect must be explained deterministically. This leads to an energetic explanation by fracture mechanics.

If linear elastic fracture mechanics (LEFM) were applicable, the mean size effect trend in Figs. 3(*b*), 6(*b*), and 9(*b*) would have to be a straight line of slope $-1/2$. However, the mean trend in these plots is obviously less steep than that. It follows that the fracture process zone (FPZ) has a non-negligible size, which causes nonlinear fracture behavior. This means that LEFM does not apply and the cohesive crack model is needed.

In our case, the cohesive fracture is a shear fracture that propagates in the foam in the immediate vicinity of the interface with the skin. Strictly speaking, it is neither mode I nor mode II fracture because, in the vicinity of the skins, neither symmetric nor antisymmetric behaviors can be defined. Nevertheless, as an approximation, it seems reasonable to assume that the fracture energy G_{fs} characterizing the fracture of foam near the skin is roughly equal to the mode II shear fracture energy G_f^{II} of foam. For most materials, G_f^{II} is many times larger than the mode I fracture energy, G_f^{I}, but for the foam, according to preliminary finite element simulations, it seems to be only about 20% larger (doubtless because of large collapsible pores).

According to the equivalent LEFM approximation of cohesive (or quasi-brittle) fracture (in which the tip of an equivalent LEFM crack is placed into the middle of the FPZ of length $2c_f$), the nominal strength of the structure may generally be expressed as [13,23,28]

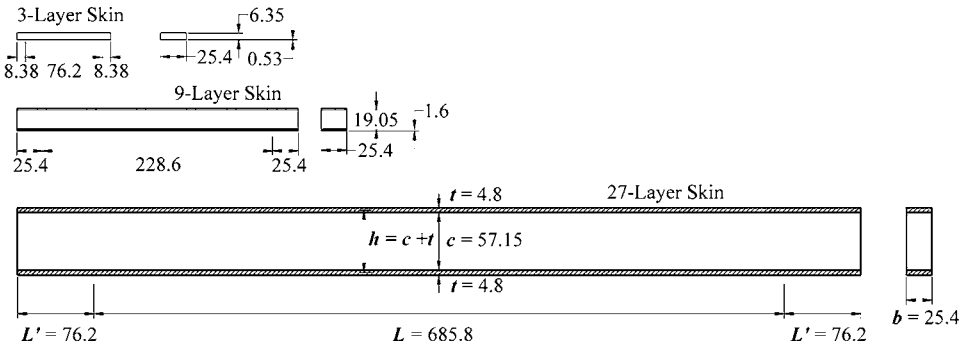

Fig. 7 Dimensions of test beams with no notches

$$\sigma_N = \sqrt{\frac{EG_{fs}}{g(\alpha)h}}, \quad \alpha = \frac{a}{h}, \quad a = a_0 + c_f \tag{2}$$

where E=Young's modulus (the material is assumed to be in a state of plane stress); a_0=length of the stress-free (or fatigued) crack at maximum load, a=total crack length at maximum load, α=relative crack length; c_f=half-length of the fracture process zone, assumed to be size-independent [13,23,28]; and $g(\alpha)$=dimensionless LEFM energy release function, calculated approximately in the Appendix (note that $g(\alpha)=[k(\alpha)]^2$ where $k(\alpha)=K_I b\sqrt{h}/P$ and K_I=stress intensity factor). As confirmed in the Appendix, the sandwich beams considered here are structures of positive geometry, which means that $g(\alpha)$ is an increasing function. In that case, the structure reaches the maximum load as soon as the FPZ is fully formed, and so a_0=length of the notch.

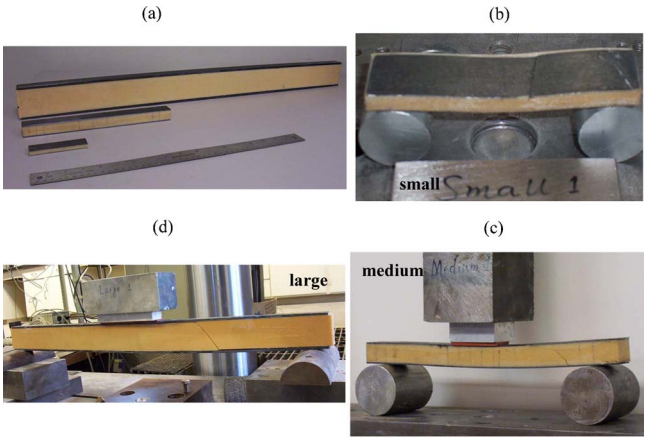

Fig. 8 (*a*) Photo of unnotched test beams of all three sizes; (*b*), (*c*), and (*d*) photo of typical failure modes for each of three beam sizes

By analogy to previous studies of size effect in quasi-brittle materials such as concrete, the maximum loads of fracture specimens and structures that are not extremely large depend only on the slope of the initial tangent of the softening curve of the cohesive crack model (or crack band model). It is logical to expect the same here. Thus, the maximum loads of the present sandwich beams depend not on the total fracture energy G_F (representing the total area under the softening curve, including its long tail), but only on the so-called initial fracture energy, which is the proper meaning of G_{fs} and represents the area under the initial tangent (Fig. 10) of the cohesive softening curve $\tau(w)$; τ=cohesive crack-bridging shear stress, w=relative displacement (or slip) between the crack faces (near the skin). In Eq. (2), we may substitute the approximation

Table 3 Data and test results for beams with no notches

No.	Depth c (mm)	Width b (mm)	Length L (mm)	Load P (N)	σ_N (MPa)	Failure modes
S1	6.35	25.4	76.23	583	3.336	Upper skin compressive failure
S2	6.35	25.4	76.23	600	3.433	Upper skin compressive failure
S3	6.35	25.4	76.23	575	3.290	Upper skin compressive failure
S4	6.35	25.4	76.23	814	4.658	Upper skin compressive failure
S5	6.35	25.4	76.23	688	3.937	Upper skin compressive failure
S6	6.35	25.4	76.23	688	3.937	Upper skin compressive failure
S7	6.35	25.4	76.23	605	3.462	Upper skin compressive failure
S8	6.35	25.4	76.23	702	4.017	Upper skin compressive failure
S9	6.35	25.4	76.23	688	3.937	Upper skin compressive failure
S10	6.35	25.4	76.23	732	4.188	Upper skin compressive failure
S11	6.35	25.4	76.23	714	4.085	Upper skin compressive failure
S12	6.35	25.4	76.23	699	3.999	Upper skin compressive failure
S13	6.35	25.4	76.23	642	3.673	Upper skin compressive failure
M1	19.05	25.4	228.6	1740	3.317	Shear fracture
M2	19.05	25.4	228.6	1698	3.237	Shear fracture
M3	19.05	25.4	228.6	1927	3.673	Shear fracture
M4	19.05	25.4	228.6	1879	3.582	Upper skin compressive failure
M5	19.05	25.4	228.6	1792	3.416	Upper skin compressive failure
M6	19.05	25.4	228.6	1756	3.347	Shear fracture
M7	19.05	25.4	228.6	2144	4.087	Upper skin compressive failure
M8	19.05	25.4	228.6	1808	3.447	Shear fracture
M9	19.05	25.4	228.6	1737	3.311	Upper skin compressive failure
L1	57.15	25.4	685.8	5864	3.726	Upper skin compressive failure
L2	57.15	25.4	685.8	5849	3.717	Upper skin compressive failure
L3	57.15	25.4	685.8	5815	3.695	Shear fracture
L4	57.15	25.4	685.8	3525	2.240	Shear fracture
L5	57.15	25.4	685.8	4809	3.056	Upper skin compressive failure

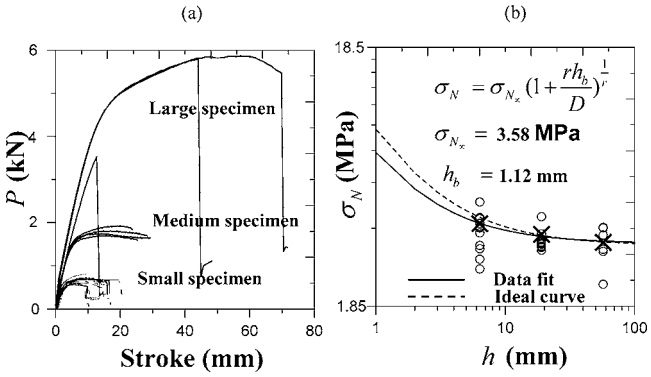

Fig. 9 (*a*) Load-deflection diagrams measured on unnotched beams of three sizes and (*b*) nominal strength values measured on these beams, compared to the size effect law for failure at crack initiation

$$g(\alpha) \approx g(\alpha_0) + g'(\alpha_0)(c_f/h) \tag{3}$$

in which $c_f/h=\alpha-\alpha_0$. This leads to the well-known size effect law

$$\sigma_N = \sqrt{\frac{EG_{fs}}{g'(\alpha_0)c_f + g(\alpha_0)h}} = \frac{\sigma_0}{\sqrt{1+h/h_0}} \tag{4}$$

where c_f=constant, approximately representing the half-length of the FPZ, and h_0 and σ_0 are constants if the notches are geometrically similar (i.e., if $\alpha=a_0/h$=constant)

$$\sigma_0 = \sqrt{EG_{fs}/c_f g'(a_0)}, \quad h_0 = c_f g'(a_0)/g(a_0) \tag{5}$$

The mechanics of bending and shear of sandwich plates may be used to obtain approximate expressions for the energy release functions $g(\alpha)$ for the test geometries considered; see the Appendix.

Having noted this theoretical background, we may check whether it can explain the experimental results. Figure 6(*b*) shows that the classical energetic size effect law in Eq. (4) can fit the nominal strength values measured on sandwich beams of series II with notches at bottom. The fit is as good as can be desired in view of the inevitable random scatter of experiments.

In Fig. 3(*b*), the classical energetic size effect law in Eq. (4) is compared to the measured values of nominal strength for series I of sandwich beams with notches on top. For this series, the fracture energy in shear is found as G_{fs}=214.1 kN/mm and the FPZ half-size turned out to be c_f=101.9 mm.

In Fig. 6(*b*), the same size effect law is used to approximate the measured values of nominal strength for test series II in which the notches were located at the bottom interface. Although the specimens of this series had a stronger skin, their depth was less than for series I specimens, and so the overall moment capacity was lower. The fracture energy in shear (near the interface) was determined to be G_{fs}=71 kN/mm, and the FPZ half-size as c_f =21.6 mm.

It must be noted that these fracture energies in shear appear to be several orders of magnitude higher than the shear fracture energy of foam alone, as estimated by preliminary finite element simulations (roughly 0.60 N/mm). This discrepancy must be explained by the composite action of the skin with very high axial stiffness. The high skin stiffness causes that (1) most of the strain energy is stored in the skin, and released from the skin, and that (2) the effective FPZ length $2c_f$ near the interface is much larger than in the foam alone [15] (see Appendix).

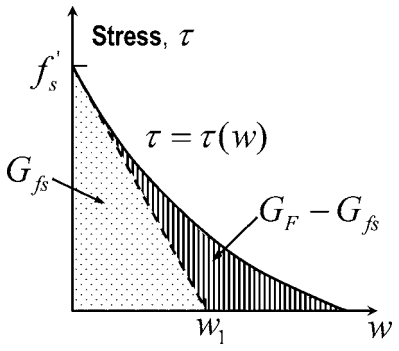

Fig. 10 Softening cohesive stress-slip curve for shear crack and its initial linear approximation

Size Effect at Crack Initiation in Unnotched Sandwich Beams

In test series III, the sandwich beams had no notches. The approximate solutions of energy release rate in the Appendix demonstrate that the sandwich beams considered have a positive geometry, and therefore reach the maximum load as soon as the fracture process zone in the skin-core interface is formed. In spite of that, the statistical Weibull-type size effect is out of the question because mechanics dictates that the fracture can initiate at only one place—very near the skin-core interface at the end of beam.

For crack initiation, we generally have $g(\alpha_0)=0$, and thus the third term of the series expansion extending $g(\alpha)$ in Eq. (3) must be included

$$g(\alpha) \approx g'(\alpha_0)(c_f/h) + \frac{1}{2}g''(\alpha_0)(c_f/h)^2 \tag{6}$$

Substituting this into (2), and modifying the resulting expression according to the required asymptotic properties without affecting the first two nonzero terms of the large-size and small-size asymptotic expansions in terms of h and h^{-1}, we obtain the well-known formula for the classical deterministic (energetic) size effect for failures at crack initiation [23,26,28,39];

$$\sigma_N = \sigma_N^\infty\left(1 + \frac{h_b}{h}\right) \tag{7}$$

in which σ_N^∞ and h_b are constants; $\sigma_N^\infty=\sqrt{EG_f/g'(0)c_f}$ and $h_b=-c_f g''(0)/4g'(0)$.

The solid curve in Fig. 9(*b*) shows the optimum fit of this formula to the data measured in test series III. For this series of tests, the shear fracture energy is determined as G_{fs} =240.4 kN/mm, and the effective half-length of FPZ as c_f =2.9 mm. Regression of size effect test data provided h_b =1.12 mm and σ_0=3.58 MPa. It must be pointed out, however, that the smallest beams failed by compressive fracture of the skins rather than shear fracture of the foam. This means that the load that would have caused failure by shear fracture of the foam must have been higher than the measured load, a fact that has been proved by preliminary finite element simulations. In Fig. 9(*b*), this would shift the data points for the smallest beams upward, as sketched by the dashed curve. thus, the true size effect must be stronger than that seen in Fig. 9(*b*). In other words, although the figure does not represent purely the size effect of shear fracture, it does represent a conservative estimate of the size effect of such fracture.

Conclusions

1. As expected on the basis of a theory previously developed for other quasi-brittle materials, failure of sandwich plates consisting of fiber composite skins and PVC foam core exhibits a significant size effect. This is true not only for notched (or damaged) sandwich structures, but also for unnotched ones.

2. The observed size effect cannot be attributed to Weibull theory of local material strength because the crack causing failure cannot form at random locations. In the notched beams tested, the material failure is forced to occur at one precise location—the notch tip—and in unnotched beams the crack seen to initiate at one precise location—the interface at the beam end. Thus, the only possible physical source of size effect is deterministic, which inevitably leads to the energetic theory.
3. Consequently, it is unrealistic to predict the load capacity of large sandwich structures based on the concept of material strength or plastic limit analysis.
4. For normal size sandwich structures, the size effect is weaker than that of linear elastic fracture mechanics (LEFM). Therefore, the use of LEFM to calculate load capacity is not realistic. Failure theories with a characteristic length, such as fracture mechanics based on the cohesive crack model, crack band model, or nonlocal damage mechanics, need to be used.
5. Similar to other quasi-brittle materials, one must distinguish two types of size effect: (1) size effect for failures-occurring at fracture initiation in an uncracked (and unnotched) structure and (2) failures due to fracture propagation from pre-existing large cracks or damage zones.
6. The formulas for the size effect on nominal strength of notched or unnotched sandwich beams, derived by asymptotic approximation based on equivalent LEFM, match the experimental results satisfactorily. Different formulas apply to beams with notches simulating pre-existing stress-free (fatigued) cracks and to unnotched beams failing at crack initiation.
7. Knowledge of the size effect formulas makes it possible to identify from size effect experiments both the fracture energy and the effective size of the fracture process zone.

Acknowledgment

Financial support from the Office of Naval Research under grant ONR-N00014-91-J-1109 to Northwestern University is gratefully acknowledged. F.C. C. acknowledges with thanks financial support from Catalan Institution for Supporting Research, AGAUR.

Appendix: Calculation of Maximum Loads of Sandwich Beams

Consider a simply supported sandwich beam of symmetric cross section, with span L, one concentrated load P at midspan, and a crack in the top interface (as in test series I). Let x be the longitudinal coordinate measured from the left support. If the beam is not notched, the theory of bending implies that such a crack should begin propagating above the support where the shear stress in the core is maximum. It is assumed that the crack propagates only inward. Let the tip of the crack be located at $x=a=\alpha h$ where α is called the dimensionless crack length and $D=h=c+t=$distance between the centers of skins; c and t are thickness of core and skin, respectively (Fig. 11(a)).

According to the standard hypothesis of plane cross sections of the core remaining plane, the bending moment distribution along the skin would have a sudden drop to zero at the notch tip. In reality, this hypothesis is locally, near the tip, far from true. thus, the moment in the skin must drop to zero gradually over a certain finite transition length, which may be assumed as

$$L_t = \eta\frac{L}{2}\left(1 - 2\alpha\frac{h}{L}\right) \tag{8}$$

The results are reasonable if η is considered to be in the range [0.01,0.3], depending on the specimen geometry and the type of size effect; L_t is measured from the crack front such that along this length the skin moment reduces to zero gradually. Introduction of this finite transition length was found to be essential for obtaining a realistic form of function $g(\alpha)$. Without a finite L_t, the complementary potential energy in Eq. (12) would yield function $g(\alpha)$ with a vanishing second derivative, which would conflict with the derivation of the size effect law for crack initiation [23–25]. The alternative of considering above the support a two-tip crack that can grow both inward and outward has also been found to be insufficient to describe the observed size effect at crack initiation. In accordance with the classical sandwich beam assumptions, the axial normal stresses in the core are neglected. So are the shear forces transmitted by the skins, with two exceptions: (1) in the cracked cross sections in which the core cannot resist any shear, and (2) along the transition length L_t, in which it is assumed that the shear is resisted by both the core and the skins (Fig. 11(b)). In addition, the crack surfaces are assumed to be free of stress.

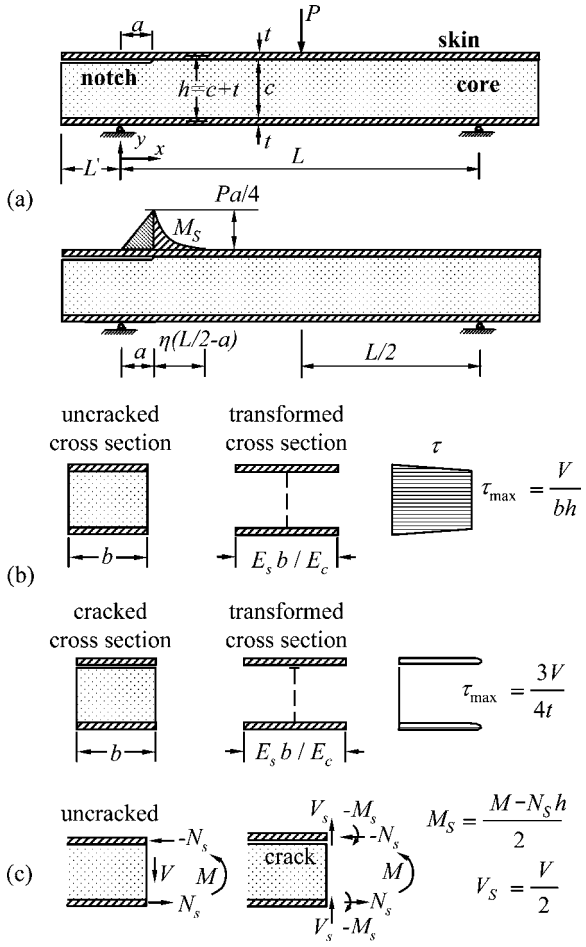

Fig. 11 Illustrations for beam-type analysis of fracture in the Appendix

Let subscript c refer to the core and subscript s to the skin; $b=$beam width; $\alpha=a/h=$dimensionless crack length measured from the support; $I=bth^2/2=$moment of inertia of sandwich cross section; and $I_s=bt^3/12$ moment of inertia of each skin. At an uncracked cross section, each skin is subjected to a normal force N_s, and a bending moment M_s; and if the section is inside the transition length, a shear force V_s, while the core sustains the total shear force if the section is uncracked, so that $V=V_c$, or part of it if it is in the transition length, but it sustains no bending moment anywhere along the beam length (see Fig. 11(c)). In a cracked cross section, on the other hand, the core receives no stress and all of the shear force and bending moment is resisted by the skins ($V_c=M_c=0$) (Fig. 11(c)).

The conditions of equilibrium of moments and horizontal forces acting on a cross section lead to the following distributions of internal forces

(i) for $0 \leqslant x \leqslant \alpha h$:

$$M_s = \frac{P}{4}x, \quad V_s = \frac{P}{4}, \quad N_s = 0, \quad V = 2V_s \tag{9}$$

(ii) for $\alpha h \leqslant x \leqslant \alpha h + L_t$:

$$M_s = \frac{P}{4}\alpha h\left(\frac{x-\alpha h}{L_t} - 1\right)^2, \quad V_s = \frac{P}{2}\alpha h\frac{x-\alpha h - L_t}{L_t^2}$$

$$N_s = \frac{Px}{2h} - \frac{P\alpha(x-\alpha h - L_t)^2}{2L_t^2}, \quad V_c = \frac{P}{2} - \frac{P\alpha h(x-\alpha h - L_t)}{L_t^2} \tag{10}$$

(iii) for $\alpha h + L_t \leqslant x \leqslant \leqslant L/2$:

$$M_s = 0, \quad N_s = \frac{Px}{2h}, \quad V_s = 0, \quad V = V_c = P/2 \tag{11}$$

From these internal forces, one can calculate the following expression for the complementary potential energy (per half beam)

$$\begin{aligned}\Pi^* = {} & \frac{2}{2E_sI_s}\int_0^{\alpha h}\left(\frac{P}{4}x\right)^2 dx + \frac{2}{2G_sbt\gamma}\int_0^{\alpha h}\left(\frac{P}{4}\right)^2 dx \\ & + \frac{2}{2E_sI_s}\int_{\alpha h}^{\alpha h + L_t}\left[\frac{P}{4}\alpha h\left(\frac{x-\alpha h}{L_t} - 1\right)^2\right]^2 dx \\ & + \frac{2}{2G_sbt\gamma}\int_{\alpha h}^{\alpha h + L_t}\left(\frac{P}{2}\alpha h\frac{x-\alpha h - L_t}{L_t^2}\right)^2 dx \\ & + \frac{2}{2E_sI}\int_{\alpha h}^{\alpha h + L_t}\left(\frac{Px}{2h} - \frac{P\alpha(x-\alpha h - L_t)^2}{2L_t^2}\right)^2 dx \\ & + \frac{1}{2G_cbh\beta}\int_{\alpha h}^{\alpha h + L_t}\left(\frac{P}{2} - \frac{P\alpha h(x-\alpha h - L_t)}{L_t^2}\right)^2 dx \\ & + \frac{2}{2E_sI}\int_{\alpha h + L_t}^{L/2}\left(\frac{Px}{2h}\right)^2 dx + \frac{1}{2G_cbh\beta}\int_{\alpha h + L_t}^{L/2}\left(\frac{P}{2}\right)^2 dx \end{aligned} \tag{12}$$

where $\beta = 1$ and $\gamma = 4/3$ are the correction factors giving the effective shear stiffness, $\beta G_c bh$ and $\gamma G_s bt$, of the core and the skin [40]. In LEFM, the energy release rate of a statically propagating crack, calculated as $\mathcal{G} = \mathcal{G}(P,a) = [\partial\Pi^*/\partial\alpha]_P/h$, must be equal to bG_{fs}; i.e.,

$$\left[\frac{\partial\Pi^*}{\partial\alpha}\right]_P = hbG_{fs} \tag{13}$$

If Eq. (13) is solved for P, one obtains for P/bD a formula of the general form of Eq. (2) in which $g(\alpha)$ is a function with parameters $h/t = 27.67$, $E_s/G_s = 6000$, $E_s/G_c = 750$, $L/t = 160$, and $L/h = 5.78$. For the sake of brevity, the resulting expression for $g(\alpha)$, which is very long, is not shown here; given the integral form of the complementary potential energy (Eq. (12)), one can calculate $g(\alpha)$ and its derivative unambiguously using any computer algebra system software.

Because the resulting expression for $g(\alpha)$ has too many terms to manage on paper, further calculations are simplified by using a third-order polynomial, obtained by fitting the numerical values of $g(\alpha)$ as shown in Fig. 12. In the calculation of numerical values of $g(\alpha)$, the parameter η is chosen to be 0.3 for test series I and II,

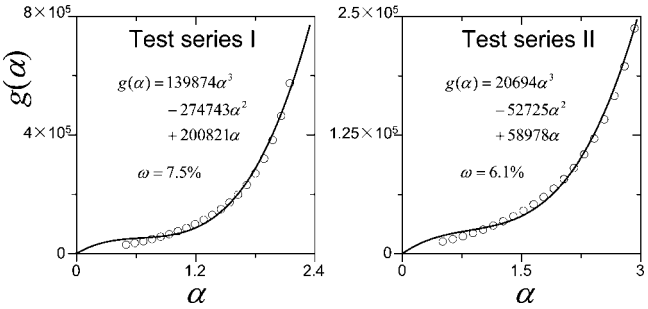

Fig. 12 Fits of the numerical values of $g(\alpha)$ for the test series I and test series II

and 0.01 for test series III, which is necessary to model the observed size effect. The polynomial fits obtained for test series I, II, and III are given by

$$g_I(\alpha) = 139874\alpha^3 - 274743\alpha^2 + 200821\alpha \tag{14}$$

$$g_{II}(\alpha) = 20694\alpha^3 - 52725\alpha^2 + 58978\alpha \tag{15}$$

$$g_{III}(\alpha) = 175176\alpha^3 - 536244\alpha^2 + 686634\alpha \tag{16}$$

Note that functions g_I, g_{II}, and g_{III} are all increasing within the range of interest. This demonstrates that the notched sandwich beam has a positive fracture geometry, and thus must fail at the start of fracture propagation if the load is controlled [28]. Further note that the second derivatives of all these functions at vanishing crack size are negative but eventually become positive at certain finite crack extension. This behavior is necessary [23–25] for explaining and modeling the size effect at crack initiation.

References

[1] Allen, H. G., 1969, *Analysis and Design of Sandwich Panels*, Pergamon Press, London.

[2] *The Handbook of Sandwich Construction*, 1997, D. Zenkert, ed., Engineering Materials Advisory Services (EMAS), Warley, UK.

[3] Gough, G. S., Elam, C. F., and De Bruyne, N. D., 1940, "The Stabilization of a Thin Sheet by Continuous Supporting Medium," J. R. Aeronaut. Soc., **44**, pp. 12–43.

[4] Goodier, J. N., and Neou, I. M., 1951, "The Evaluation of Theoretical Critical Compression in Sandwich Plates," J. Aeronaut. Sci., **18**, pp. 649–657.

[5] Hansen, U., 1998, "Compression Behavior of FRP Sandwich Specimens With Interface Debonds," J. Compos. Mater., **32**(4), pp. 335–360.

[6] Hunt, G. W., and de Silva, and L. S., 1990, "Interactive Bending Behavior of Sandwich Beams," ASME J. Appl. Mech., **57**, pp. 189–196.

[7] Pearce T. R. A., and Webber J. P. H.1972, "Buckling of Sandwich Panels With Laminated Faceplates," Aeronaut. Q., **23**, pp. 148–160.

[8] Plantema, F. J., 1966, *Sandwich Construction. The Bending and Buckling of Sandwich Beams, Plates and Shells*, Wiley & Sons, New York.

[9] Triantafillou, T. C., and Gibson, L. G., 1987, "Failure Mode Maps for Foam Core Sandwich Beams," Mater. Sci. Eng., **95**, pp. 37–53.

[10] Hunt, G. W., and Wadee, M. A., 1998, "Localization and Mode Interaction in Sandwich Structures," Proc. R. Soc. London, **454**, pp. 1197–1216.

[11] Bažant, Z. P., Daniel, I. M., and Li, Z., 1996, "Size Effect and Fracture Characteristics of Composite Laminates," ASME J. Eng. Mater. Technol., **118**(3), pp. 317–324.

[12] Bažant, Z. P., Kim, J.-J. H., Daniel, I. M., Becq-Giraudon, E., and Zi, G., 1999, "Size Effect on Compression Strength of Fiber Composites Failing by Kink Band Propagation," Int. J. Fract., **95**, pp. 103–141.

[13] Bažant, Z. P., Zhou, Y., Novák, D., and Daniel, I. M., 2004, "Size Effect on Flexural Strength of Fiber-Composite Laminate," ASME J. Eng. Mater. Technol., **126**, pp. 29–37.

[14] Bažant, Z. P., 2002, "Size Effect Theory and Its Application to Fracture of Fiber Composites and Sandwich Plates," *Continuum Damage Mechanics of Materials and Structures*, O. Allix and F. Hild, eds., Elsevier, Amsterdam, pp. 353–381.

[15] Bažant, Z. P., Zhou, Y., Zi, G., and Daniel, I. M., 2003, "Size Effect and Asymptotic Matching Analysis of Fracture of Closed-Cell Polymeric foam," Int. J. Solids Struct., **40**, pp. 7197–7217.

[16] Brocca, M., Bažant, Z. P., and Daniel, I. M., 2001, "Microplane Model for Stiff Foams and Finite Element Analysis of Sandwich Failure by Core Indentation," Int. J. Solids Struct., **38**, pp. 8111–8132.

[17] Daniel, I. M., Gdoutos, E. E., Wang, K.-A., and Abot, J. L., 2002), "Failure Modes of Composite Sandwich Beams," Int. J. Damage Mech., **11**(4), pp.

309–334.
[18] Bayldon, J., Bažant, Z. P., Daniel, I. M., and Yu, Q., 2006, "Size Effect on Compressive Strength of Laminate-Foam Sandwich Plates," ASME J. of Materials and Technology, 128, in press.
[19] Gdoutos, E. E., Daniel, I. M., Wang, K.-A., and Abot, J. L., 2001, "Nonlinear Behavior of Composite Sandwich Beams in Three-Point Bending," Exp. Mech., **41**, pp. 182–188.
[20] Zenkert, D., 1990, "Strength of Sandwich Beams With Mid-Plane Debondings in the Core," Compos. Struct., **15**(4), pp. 279–299.
[21] Zenkert, D., 1991, "Strength of Sandwich Beams With Interface Debondings," Compos. Struct., **17**(4), pp. 331–350.
[22] Bažant, Z. P., 1984, "Size Effect in Blunt Fracture: Concrete, Rock, Metal," J. Eng. Mech., **110**(4), pp. 518–535.
[23] Bažant, Z. P., 2002, *Scaling of Structural Strength*. Hermes Penton Science (Kogan Page Science), London (also: French translation with updates, Hermes, Paris, 2004).
[24] Bažant, Z. P., 2004, "Scaling Theory for Quasibrittle Structural Failure," Proc. of the National Academy of Sciences, in press.
[25] Bažant, Z. P., 1997, "Scaling of Quasibrittle Fracture: Asymptotic Analysis," Int. J. Fract., **83**(1), pp. 19–40.
[26] Bažant, Z. P., and Chen, E.-P., 1997, "Scaling of Structural Failure," Appl. Mech. Rev., **50**(10), pp. 593–627.
[27] Bažant, Z. P., and Kazemi, M. T., 1990, "Size Effect in Fracture of Ceramics and Its Use to Determine Fracture Energy and Effective Process Zone Length," J. Am. Ceram. Soc., **73**(7), pp. 1841–1853.
[28] Bažant, Z. P., and Planas, J., 1998, *Fracture and Size Effect in Concrete and Other Quasibrittle Materials*, CRC Press, Boca Raton, FL.
[29] RILEM Committee QFS, 2004, "Quasibrittle Fracture Scaling and Size Effect—Final Report," Mater. Struct. **37**(272), pp. 547–586.
[30] Benson, A. S., and Mayers, J., 1967, "General Instability and Face Wrinkling of Sandwich Plates—Unified Theory and Applications," AIAA J., pp. 729–739.
[31] Cheng, S.-H., Lin, C.-C., and Wang, J. T.-S., 1997, "Local Buckling of Delaminated Sandwich Beams Using Continuous Analysis," Int. J. Solids Struct., **34**(2), pp. 275–288.
[32] Gdoutos, E. E., Daniel, I. M., and Wang, K.-A., 2003, "Compression Facing Wrinkling of Composite Sandwich Structures," Mech. Mater., **35**(3–6), pp. 511–522.
[33] Hadi, B. K., and Matthews, F. L., 2000, "Development of Benson-Mayers Theory on the Wrinkling of Anisotropic Sandwich Panels," Comput. Struct., **49**, pp. 425–434.
[34] Hoff, N. J., and Mautner, S. E., 1945, "The Buckling of Sandwich-Type Panels," J. Aeronaut. Sci., **12**, pp. 285–297.
[35] Heath, W. G., 1960, "Sandwich Construction. Part 2: The Optimum Design of Flat Sandwich Panels," Aircr. Eng., **31**, pp. 230–235.
[36] Stifflinger, M. A., and Rammerstorfer, F. G., 1997, "Face-Layer Wrinkling in Sandwich Shells—Theoretical and Experimental Investigations," Thin-Walled Struct., **29**, pp. 113–127.
[37] Vonach, W. K., and Rammerstorfer, F.-G., 2000, "The Effect of In-plane Core Stiffness on the Wrinkling Behavior of Thick Sandwiches," Acta Mech., **141**, pp. 1–10.
[38] Bažant, Z. P., and Cedolin, L., 2003, *Stability of Structures: Elastic, Inelastic, Fracture and Damage Theories*, 2nd ed., Dover, New York.
[39] Bažant, Z. P., and Li, Z., 1996, "Zero-Brittleness Size-Effect Method for One-Size Fracture Test of Concrete," J. Eng. Mech., **122**(5), pp. 458–468.
[40] Timoshenko, S. P., and Goodier, J. N., 1987, *Theory of Elasticity*, 3rd ed. McGraw-Hill, New York.